GEOPHYSICAL RESEARCH LETTERS, VOL. 33, L24308, doi:10.1029/2006GL028005, 2006

The 17 July 2006 Java tsunami earthquake

Charles J. Ammon,[1] Hiroo Kanamori,[2] Thorne Lay,[3] and Aaron A. Velasco[4]

Received 2 September 2006; revised 5 November 2006; accepted 14 November 2006; published 22 December 2006.

[1] The 17 July 2006 Java earthquake involved thrust faulting in the Java trench and excited a deadly tsunami (~5–8 m) that inundated the southern coast of Java. The earthquake's size estimates vary significantly with seismic wave period: very long-period signals (300–500+ s) indicate a seismic moment of 6.7×10^{20} Nm (M_w = 7.8), M_S (~20 s) = 7.2, m_b (~1 s) = 6.2, while shaking intensities (3–10 Hz) were $\leq$ MMIV. The large tsunami relative to M_S characterizes this event as a tsunami earthquake. Like previous tsunami earthquakes, the Java event had an unusually low rupture speed of 1.0–1.5 km/s, and occurred near the up-dip edge of the subduction zone thrust fault. Most large aftershocks involved normal faulting. The rupture propagated ~200 km along the trench, with several pulses of shorter period seismic radiation superimposed on a smooth background rupture with an overall duration of ~185 s. **Citation:** Ammon, C. J., H. Kanamori, T. Lay, and A. A. Velasco (2006), The 17 July 2006 Java tsunami earthquake, *Geophys. Res. Lett.*, *33*, L24308, doi:10.1029/2006GL028005.

1. Introduction

[2] The 17 July 2006 Java earthquake (NEIC: 9.26°S, 107.39°E; 08:19:28 UTC) involved compressional faulting at shallow depth in the Java trench (Figure 1). The shallow dipping (thrust) plane fits the down-dip width of the aftershock distribution better than the steep plane and we assume that slip occurred along this surface. The event was felt on Java with peak intensity of only MMIV in Bandung, Jakarta, Pangandaran, and Tasikmalaya (all more than 150 km from the source), but loss of life was high (637 killed, 164 missing) (http://earthquake.usgs.gov/eqcenter/eqinthenews/2006/usqgaf/#summary) due to a tsunami with 5–8 m run-up amplitudes along the southern coast of central Java from Ciandum to Yogyakarta (Y. Tsuji, personal communication, 2006). The event's seismic magnitudes (m_b = 6.2; M_S = 7.2; M_w = 7.2 (~25 s body waves - USGS); M_w = 7.7 (~150 s surface waves – Global CMT)), indicate an increase in apparent source strength with increasing period, and we estimate a seismic moment of 6.7×10^{20} N-m (M_w = 7.8) for very long period (300–500+s Rayleigh waves). The large size of the tsunami relative to the M_S value classifies this earthquake as a tsunami earthquake [*Kanamori*, 1972].

[3] We analyze Rayleigh and body waves of the 2006 Java event and find that rupture was unusually long (~185 s) and propagated slowly (1.0–1.5 km/s), attributes shared with other tsunami earthquakes [*Polet and Kanamori*, 2000; *Lay and Bilek*, 2006]. The 2 June 1994 (M_w = 7.8) Java earthquake, located about 600 km east-southeast of the 2006 event, had similar strong tsunami excitation (13.9 m maximum run-up height [*Tsuji et al.*, 2005]), and both events have aftershock sequences dominated by normal faulting, suggesting relatively complete stress release on the interplate thrust [e.g., *Abercrombie et al.*, 2001; *Polet and Thio*, 2003]. We show that the 2006 Java earthquake involved 5 to 6 pulses of moment release superimposed on a smooth rupture, indicating a compound frictional environment likely influenced by weak material properties related to sediment subduction or the presence of fluids [e.g., *Kanamori and Kikuchi*, 1993].

2. Surface-Wave Source Time-Function Analysis

[4] The 17 July 2006 Java earthquake provided several hundred global broadband seismic recordings, with well-excited long-period surface waves. We first analyze long-period Rayleigh wave signals to characterize the overall rupture properties. The instrument responses were removed and a frequency-domain taper applied to the ground displacement observations with a cutoff at a period of 800 s and a corner at 750 s. We computed point-source synthetic seismograms (theoretical Green's functions: TGFs) using normal-mode summation (down to 30 s period) for PREM [*Dziewonski and Anderson*, 1981] for the NEIC epicentral location, a depth of 15 km, and a faulting geometry (strike: 289°; dip: 10°; rake: 95°) as determined by the Global CMT project (Figure 1). The dip is shallow, but not constrained precisely; assuming a shallower dip produces a larger seismic moment estimate. The TGFs were deconvolved from the corresponding observations, to obtain effective source time functions (STFs) for the surface wave signals in designated time windows [*Ammon et al.*, 2005].

[5] For each station, we isolated long-period minor-arc Rayleigh waves (R1) using a group-velocity range of 8 km/s to either 2.75 km/s or the start of the major-arc Rayleigh waves (R2) as defined by 5 km/s velocity. This long time window captures some body waves, but this is negligible for extracting first-order rupture characteristics because the surface wave energy completely dominates the signal. We removed the mean and tapered the signals, then deconvolved the TGF using both water-level deconvolution and iterative time-domain procedures [*Kikuchi and Kanamori*, 1982]. A unit-area low-pass Gaussian filter with a full-width at half the maximum of 32 s was convolved with the result

[1]Department of Geosciences, Pennsylvania State University, State College, Pennsylvania, USA.
[2]Seismological Laboratory, California Institute of Technology, Pasadena, California, USA.
[3]Department of Earth and Planetary Sciences, University of California, Santa Cruz, California, USA.
[4]Department of Geological Sciences, University of Texas at El Paso, El Paso, Texas, USA.

0094-8276/06/2006GL028005$05.00

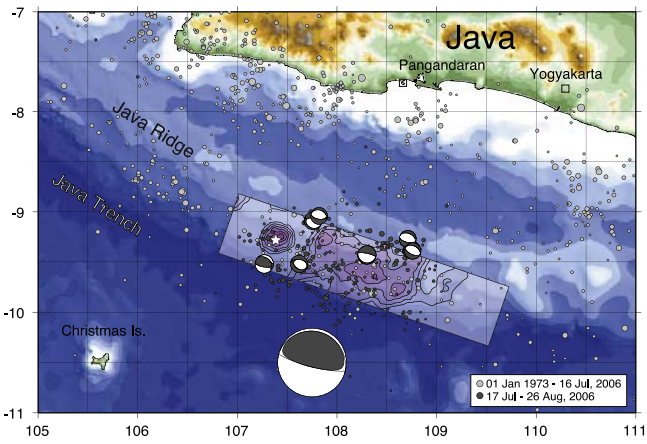

Figure 1. Map showing the Global CMT solutions for the 17 July 2006 Java tsunami earthquake and aftershocks and the NEIC epicenters of mainshock (star), aftershocks (dark circles), and prior activity (gray circles). The mainshock CMT solution is centered near the centroid location, which has a bias toward the southwest; other CMTs are at the NEIC locations. The preferred slip model found in this paper is contoured (scale is shown in Figure 4).

to reduce the influence of short-period signals that are more sensitive to the assumed source depth, focal mechanism, and propagation errors in the TGF. The iterative approach allows control on the STF causality and positivity, so we focus our analysis on corresponding results. The recovered period range extends from about 50 to 750 s. Figure S1 (see auxiliary material[1]) shows an example surface wave STF estimation.

[6] The STFs were screened to insure that their convolution with the TGF produces at least a 70% fit to the observed vertical displacement, which excludes most of the problematic deconvolutions. We also visually inspected the observations and the STFs to identify unstable solutions and to eliminate stations with obvious gain problems. Some of the remaining time functions contained incoherent very long-period (> 750 s period) noise starting some time after the main pulse in the deconvolutions. This long-period noise varies between nearby stations and depends on the deconvolution window length. In contrast, the main STF pulse is robust. We performed our source analysis restricting our attention to the dominant time function pulse, which we believe represents the actual rupture process.

[7] The Rayleigh wave STFs are shown in Figure 2 as a function of directivity parameter, $\Gamma = \cos(\theta - \theta_r)/c$, where θ is the azimuth of the station, θ_r is the rupture direction (here specified as 109°N, which proves optimal), and c is a reference phase velocity, assumed to be 3.8 km/s. All the time functions are between 100 and 200 s in duration, and there is a clear trend toward shorter time functions for positive Γ, indicating a roughly eastward propagating rupture, consistent with the aftershock distribution (Figure 1). A number of STFs have early onsets and most of these are for paths to the south. The cause could be aspherical path effects or effects of source geometry or near-source structure. We observe about 80–100 s of directivity. For a simple, unilateral fault rupture, the maximum directivity is $2L/c$, where L is the rupture length and c is the wave phase velocity. Using c = 3.8 km/s, the observations suggest a rupture length on the order of 190 km. Assuming a 190 km rupture and a total event duration of about 150 s suggests a mean rupture speed of about 1.27 km/s. Bilateral effects can complicate this analysis, and we explore more sophisticated models below.

[8] We estimate the seismic moment by integrating 207 R1 STFs (Figure S2). The result, $M_o = 6.7 \times 10^{20}$ Nm, is about 60% larger than the Global CMT estimate (4.0×10^{20} Nm). The CMT estimate is based on surface waves with periods of roughly 100–200 s, and an assumed triangle source time function with a duration of 100 s. Our result is based on data with periods of up to about 500 s. We averaged the amplitude spectra computed for the R1 STFs to characterize the long period source spectrum. No azimuthal weighting was used, so the result may be slightly biased towards western North America (azimuth ~30–60°), where we have a large number of observations. Figure 3 shows the mean STF amplitude spectrum, and the spectrum incorporated into the global CMT solution. We also show a reference ω-squared source spectrum for a typical stress drop of 3 MPa and the same seismic moment. Our spectral amplitudes are consistent with the CMT spectrum within a factor of two in the passband emphasized in the CMT analysis. The source spectrum has a steeper long-period slope than the triangle spectrum assumed in the CMT modeling and has a larger seismic moment. The source spectrum estimated from broadband body waves signals is also shown in Figure 3, and it is clear that the overall spectrum is compound, effectively having two corner frequencies. Apparently, high-frequency radiation originated from localized regions of the rupture, long-period wave excitation originated from the entire rupture.

3. Broadband Fault Rupture Imaging

[9] We used a search-based algorithm [*Velasco et al.*, 2000; *Ammon et al.*, 2006] to estimate a smooth moment distribution that matches observed R1 STFs and teleseismic

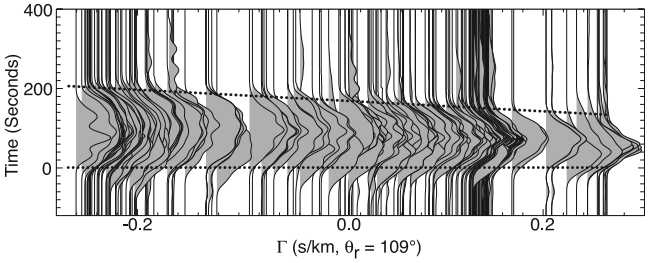

Figure 2. Rayleigh wave STFs for the 17 July 2006 Java earthquake plotted as a function of directivity parameter, Γ, assuming a rupture propagating at an azimuth of N109°E. STFs corresponding to rupture towards the station are located on the right, those in a direction away from rupture are on the left. The time functions systematically decrease in width from 200 s to 100 s as Γ increases from left to right, as indicated by the dotted lines.

[1]Auxiliary materials are available in the HTML. doi:10.1029/2006GL028005.

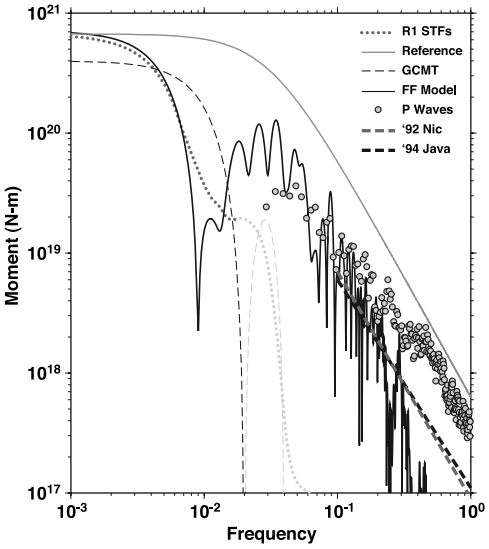

Figure 3. Spectrum of the moment rate function from the finite fault inversion (FF), the average R1 STF amplitude spectrum, the Global CMT assumed time function spectrum, and average values for the P wave spectrum computed using the method of *Polet and Kanamori* [2000]. The R1 and GCMT spectra are light gray where they are extrapolated to short periods. An average ω-squared source spectrum with typical corner frequency is shown for reference. The average P wave spectra for the 1992 Nicaragua and 1994 Java tsunami earthquakes are also shown.

P and SH waveforms in a least-squares sense. In the local–search algorithm, the rupture model is successively perturbed in a search for better fitting models. We use a zero-slip initial model and include several thousand perturbations. The inversion is parameterized in terms of point-source strength, which we convert to slip by assuming each point source represents a subevent with dimensions equal to the distance between sources (5 km) and a shear modulus, μ = 10 GPa. The time function of each subfault is that used by *Ji et al.* [2002], with a duration parameter that was allowed to vary between 8, 12, and 16 s. For the STFs, the mechanism and depth of each point source in the model are assumed to be identical to those specified in the STF estimation. Numerical experiments suggest that the main limitations from ignoring depth variations in the STF computations are relatively small amplitude, low frequency artifacts in the STF estimates which are not of major concern for estimating first-order rupture characteristics [e.g., *Ammon et al.*, 2006]. The mechanism is also fixed for P-waveform computation, but the depth is adjusted along the 10° dipping plane. We explored variable rake models using P waveforms and found the rake to be stable across the rupture. We used body-waves from distant stations to minimize PP and SS interference and corrected each waveform for geometric spreading to a uniform distance of 60°. We assume a simple water-layer over a half-space near-source velocity structure with P- and S-wave velocities of 6.70 km/s and 3.87 km/s, respectively.

[10] The spatial slip distribution varies with rupture speed in an intuitive manner; higher speed results in a larger spatial spread of slip, and lower speed produces more spatially concentrated slip distributions. Direct constraint on rupture-speed is limited. The directivity in the STFs is consistent with finiteness of less than 250 km with rupture velocities less than 1.5 km/s (larger rupture velocities predict stronger azimuthal variations). High frequency P wave back-projection favors rupture velocities of about 1 km/s (J. Mori, personal communication, 2006). We initially assumed a large, 400 × 100 km^2 fault surface, but most slip was concentrated in the upper 40 km of the fault and east of the hypocenter. For our final inversions we reduced the fault width to 75 km.

[11] Figure 4 (top) includes a slip model for an assumed rupture velocity of 1.25 km/s. The hypocenter (0,0) is located at the NEIC epicenter at a depth of about 7 km. The peak moment for the subfaults is 0.34 × 10^{20} N-m and the total moment is 7.0 × 10^{20} N-m, (M_w = 7.8), slightly higher than our preferred moment estimated from the total set of STFs. Our assumption of μ = 10 GPa is consistent with sedimentary material within the accretionary wedge [e.g., *Kopp and Kukowski*, 2003], and gives an average slip of about 8 m and peak slip just under 14 m. The slip magnitude scales inversely with μ; average slip values of 8 to 15 m are compatible with the 5–8 m run-up on Java (S. Ward, personal communication, 2006). Five to six patches of large slip are suggested, initial slip near the hypocenter at just over 10 km depth, and other slip concentrations about 50, 110, 150, and 200 km to the east. The localized asperities are constrained primarily by the body waveforms; the R1 STFs constrain the overall rupture spatial dimensions and the smoother components of slip. The majority of the well-constrained slip is at depths of 7 to 8 km to the east of the hypocenter; the total rupture length is about 170–200 km. This rupture dimension is consistent with tsunami source area estimates (Y. Fujii and K. Satake, Tsunami source of the July 2006 south off Java earthquake estimated from tide gauge records, submitted to *Geophysical Research Letters*, 2006). The moment rate function (Figure 4, bottom) contains pulses associated with each of the asperities, and is robustly resolved, with little dependence on assumed rupture velocity. The total rupture duration is about 185 s. This duration is consistent with estimates from back-projection of short-period signals (S. Ni, personal communication, 2006). Fits of the predictions for this model to the corresponding body waves and STFs are shown in Figure 5; comparable fits to the very broadband data are obtained for models with rupture velocities from 1.0 to 1.5 km/s.

4. Discussion and Conclusion

[12] Tsunami earthquakes were originally defined by *Kanamori* [1972] as events that excite unusually large tsunami for their body and surface-wave magnitudes and exhibit a notable discrepancy between M_S and M_W. The 17 July 2006 Java earthquake fits most of the tsunami earthquake characteristics outlined by *Polet and Kanamori* [2000] – the rupture was centered far from the coast (Figure 1), propagated up-dip and slowly, with a relatively long duration. Tsunami earthquakes present special challenges to tsunami warning operations that motivate use of long-period seismic waves for robust assessment of total seismic moment and tsunami excitation potential.

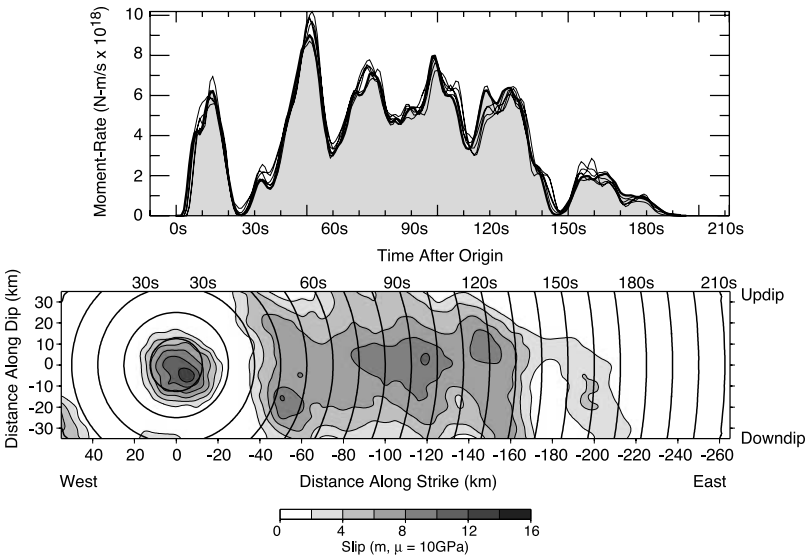

Figure 4. (top) Moment rate functions estimated from 6 finite fault inversions with rupture speeds of 1.00, 1.25, and 1.50 km/s and with and without SH waveforms. The moment-rate function is the perhaps best-constrained quantity from this type of inversion. The thicker line and shading highlight the moment-rate function from the model above. (bottom) Finite-fault inversion results for an assumed rupture speed of 1.25 km/s. The peak moment in the 5 km $\times$ 5 km cells is 0.34×10^{20} N-m and the total moment is 7.0×10^{20} N-m, (M_w = 7.8). The hypocenter location is (0, 0), the top of the fault is one km beneath the trench. Rupture front isochrons are shown at 10 s intervals (top axis); the left and bottom axes show distance from the focus in km. Slip is scaled from moment using μ = 10 GPa.

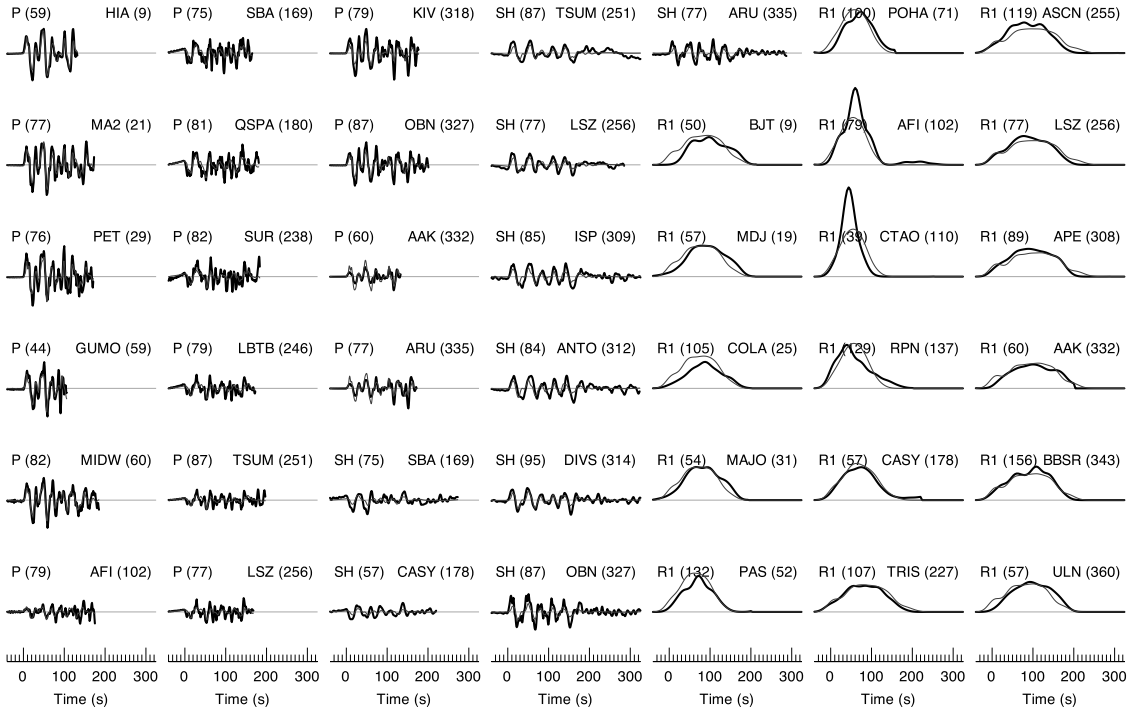

Figure 5. Observations and predictions from 16 P waveforms, 9 SH waveforms, and 17 R1 STFs used in the finite fault inversion with a rupture velocity of 1.25 km/s shown in Figure 4. Wave type and distance (°) are shown above and to the left of each waveform, the station name and azimuth (°) are shown to the right. Body waves are cut to exclude PP or SS arrivals, but no effort is made to account for core reflections. The observations are shown with a thicker black line, the predictions with the thinner gray. Observed peak STF amplitudes in the AFI and CTAO are high (as indicated by their seismic moments) because their azimuths are near a radiation node and they are sensitive to the assumed faulting geometry.

The 2 September 1992 Nicaragua earthquake (11.74°N, 87.34°W; 00:16:01.69 UTC) was a comparable seismic moment tsunami earthquake (see review by *Lay and Bilek* [2006]) and its magnitude estimates also showed a large range with $m_b = 5.3$; $M_S = 7.2$; $M_w = 7.6$ (< 150 s surface waves – CMT). The Nicaragua rupture propagated for about 100–120 s with rupture speeds $\leq$ 1.5 km/s. The Java earthquake rupture duration was significantly longer; in fact, the moment scaled-source duration for the 2006 Java event is the longest among available estimates for shallow thrust events. Although the July 2006 Java earthquake's $M_W - m_b$ difference indicates relatively low short-period body-wave radiation, the Nicaragua event radiated even less short-period energy, as did the 1994 Java event (Figure 3). We obtain a seismic energy of $E_R = 1.7 \times 10^{15}$ J from the body waves for the 2006 event, which gives an E_R/M_o ratio of 2.5×10^{-6}, a low value typical of tsunami earthquakes [*Venkataraman and Kanamori*, 2004].

[13] The occurrence of large abrupt strain release in the shallowest portions of subduction zone megathrusts raises the long-standing problem of the nature of the frictional contact in this depth range. A number of parameters can affect the shallow megathrust frictional environment, including sediment thickness, composition, fluid content and hydrologic properties, and bathymetric irregularities. The precise influence of these quantities on earthquake rupture propagation is not well known, but a reasonable assumption is that the existence of sediments along the megathrust is related to the relatively slow rupture propagation and large slip of larger and moderate-size shallow megathrust earthquakes [*Kanamori and Kikuchi*, 1993; *Bilek and Lay*, 2002].

[14] The compound nature of the Java source spectrum (Figure 3) and slip model (Figure 4) suggest that the rupture surface involved localized patches of relatively strong unstable friction surrounded by regions of either conditional stability [e.g., *Bilek and Lay*, 2002] or low frictional strength material like that which seems to have dominated the 1992 Nicaragua event. Without the impediment of the asperities, this region of the megathrust may have relieved strain through more continuous creep processes. We note that localized gravity highs in the vicinity of the rupture zone may correspond to localized changes in coupling on the megathrust (Figure S3). If we alternatively consider the rupture process in the context of fracture mechanics, the patchiness of the rupture suggests a variable specific fracture energy, G_C, distribution, with low rupture speed and creep in high G_C environments, and high rupture speed, brittle behavior in low G_C environments. Seismic data are not yet sufficient to directly resolve correlation between areas of larger slip and changes in the rupture speed to explore this context in greater depth.

[15] **Acknowledgments.** We thank Kenji Satake and an anonymous reviewer for their comments. We also thank the developers of GMT and SAC, and the seismic network operators who have constructed a superb open-data-access network for seismic research and monitoring. The facilities of the IRIS Data Management System were used to access the data used in this study. Supported by NSF grant EAR01235595 (TL) and USGS award 05HQGR0174 (CJA).

References

Abercrombie, R. E., M. Antolik, K. Felzer, and G. Ekström (2001), The 1994 Java tsunami earthquake: Slip over a subducting seamount, *J. Geophys. Res.*, *106*, 6595–6607.

Ammon, C. J., et al. (2005), Rupture process of the 2004 Sumatra-Andaman earthquake, *Science*, *308*, 1133–1139.

Ammon, C. J., A. A. Velasco, and T. Lay (2006), Rapid estimation of first-order rupture characteristics for large earthquakes using surface waves: 2004 Sumatra-Andaman earthquake, *Geophys. Res. Lett.*, *33*, L14314, doi:10.1029/2006GL026303.

Bilek, S. L., and T. Lay (2002), Tsunami earthquakes possibly widespread manifestations of frictional conditional stability, *Geophys. Res. Lett.*, *29*(14), 1673, doi:10.1029/2002GL015215.

Dziewonski, A. M., and D. L. Anderson (1981), Preliminary reference Earth model, *Phys. Earth Planet. Inter.*, *25*, 297–356.

Ji, C., et al. (2002), Source description of the 1999 Hector Mine, California, earthquake; part I: Wavelet domain inversion theory and resolution analysis, *Bull. Seismol. Soc. Am.*, *92*, 1192–1207.

Kanamori, H. (1972), Mechanism of tsunami earthquakes, *Phys. Earth Planet. Inter.*, *6*, 246–259.

Kanamori, H., and M. Kikuchi (1993), The 1992 Nicaragua earthquake: A slow tsunami earthquake associated with subducted sediments, *Nature*, *361*, 714–716.

Kikuchi, M., and H. Kanamori (1982), Inversion of complex body waves, *Bull. Seismol. Soc. Am.*, *72*, 491–506.

Kopp, H., and N. Kukowski (2003), Backstop geometry and accretionary mechanics of the Sunda margin, *Tectonics*, *22*(6), 1072, doi:10.1029/2002TC001420.

Lay, T., and S. Bilek (2006), Anomalous earthquake ruptures at shallow depths on subduction zone megathrusts, in *The Seismogenic Zone of Subduction Thrust Faults*, edited by T. H. Dixon and C. Moore, Columbia Univ. Press, in press.

Polet, J., and H. Kanamori (2000), Shallow subduction zone earthquakes and their tsunamigenic potential, *Geophys. J. Int.*, *142*, 684–702.

Polet, J., and H. K. Thio (2003), The 1994 Java tsunami earthquake and its "normal" aftershocks, *Geophys. Res. Lett.*, *30*(9), 1474, doi:10.1029/2002GL016806.

Tsuji, Y., et al. (2005), Field survey of the East Java earthquake and tsunami of June 3, 1994, *Pure Appl. Geophys.*, *144*, 839–854.

Velasco, A. A., C. J. Ammon, and S. L. Beck (2000), Broadband source modeling of the November 8, 1997, Tibet (M_w = 7.5) earthquake and its tectonic implications, *J. Geophys. Res.*, *105*, 28,065–28,080.

Venkataraman, A., and H. Kanamori (2004), Observational constraints on the fracture energy of subduction zone earthquakes, *J. Geophys. Res.*, *109*, B05302, doi:10.1029/2003JB002549.

C. J. Ammon, Department of Geosciences, Pennsylvania State University, State College, PA 16802, USA. (cammon@geosc.psu.edu)

H. Kanamori, Seismological Laboratory, California Institute of Technology, 1200 East California Blvd., Pasadena, CA 91125, USA.

T. Lay, Department of Earth and Planetary Sciences, University of California, 1156 High St., Santa Cruz, CA 95064, USA.

A. A. Velasco, Department of Geological Sciences, University of Texas at El Paso, El Paso, TX 79968-0555, USA.